Int. J. Exp. Path. (2005), 86, 297–307

ORIGINAL ARTICLE

Evaluation of human knee meniscus biopsies with near-infrared, reflectance confocal microscopy. A pilot study

Vanessa Campo-Ruiz*‡, Dinesh Patel†, R. Rox Anderson*, Emilio Delgado-Baeza‡ and Salvador González*

*Wellman Laboratories of Photomedicine, Massachusetts General Hospital, Harvard University, Boston, MA, USA, †Department of Orthopaedic Surgery, Massachusetts General Hospital, Harvard University, Boston, MA, USA, and ‡Orthopaedic Research Unit, Department of Morphology-Histology, School of Medicine, Universidad Autónoma de Madrid, Madrid, Spain

INTERNATIONAL JOURNAL OF EXPERIMENTAL PATHOLOGY

Received for publication:
16 July 2004
Accepted for publication:
4 May 2005

Correspondence:
Salvador González, MD, PhD
Assistant Professor of Dermatology
Wellman Laboratories of Photomedicine
Massachusetts General Hospital
BHX 630, 55 Fruit Street
Boston, MA 02114
USA
Tel.: +1 617 7241915;
Fax: +1 617 7262075;
E-mail: sgonzalez3@partners.org

Summary

Knee cartilage biopsy is used to confirm the pathology in both clinical and experimental conditions and often guides diagnosis and therapeutic strategies. Current histopathological techniques are time consuming, induce tissue artefacts and often prevent further evaluation, once the tissue has been fixed. Hence, there is a potential need for a fast and nondestructive imaging technique for unfixed tissue. Near-infrared, reflectance confocal microscopy (CM) allows real-time, virtual sectioning of unstained, bulk tissue samples. This pilot study evaluates the use of CM in the assessment of meniscus histopathology in a series of 26 freshly-excised human meniscus samples compared to standard light microscopy of stained sections. CM images of the meniscus show cell and matrix detail, depicting morphologic features of collagen and elastic fibres, vessels and nerve endings. In addition, crystal deposits of gout and pseudogout are also demonstrable. Thus, CM is a novel imaging technique that could enable the pathologist to make a rapid microscopic evaluation of cartilage in a fresh and unfixed fashion.

Keywords
cartilage, human meniscus, knee, laser confocal microscopy

The direct study of cartilage architecture is an essential step in the assessment of its physiology and disease. In particular, the diagnosis of knee meniscus pathology often relies on clinical examination, noninvasive imaging findings and identification of the characteristic features on histology sections (Greis *et al.* 2002). Current noninvasive imaging techniques applied to knee meniscus, such as magnetic resonance imaging, provide gross morphological features insufficient for assessing histological detail. On the other hand, evaluation of biopsy material by routine histological procedures is time-consuming, may introduce unwanted artefacts and sometimes requires specific procedures to preserve particular tissue components. Frozen sections stand as an alternative to rapidly study the tissue but induce a degree of distortion that often makes diagnosis difficult. Thus, there is a need for high-resolution imaging of human meniscus in a rapid, nondestructive fashion which is relatively free of artefacts.

Near-infrared, reflectance confocal microscopy (CM) is an imaging technique that allows virtual sectioning of bulk

tissues by illuminating a small spot within the tissue and detecting single back-scattered photons coming from the plane of interest (Wilson 1990; Pawley 1995; Rajadhyaksha *et al.* 1995; Rajadhyaksha *et al.* 1999). High-resolution optical sections are achieved by means of one or more pinholes placed in an optical conjugated plane, with a focal spot inside the tissue, so that light coming from out-of-focus planes is rejected. CM achieves a greater penetration depth inside bulk tissue specimens and provides images, in which the contrast between structures is because of natural variations in their refractive indices, so that no fluorescent stains are needed (Rajadhyaksha *et al.* 1995).

The aim of this study was to evaluate the potential of CM as an imaging tool for providing immediate microscopic information on a series of freshly-excised human knee menisci compared to conventional light microscopy of fixed sections.

Materials and methods

Human tissue specimens

Twenty-six human knee meniscus specimens were obtained under the approval of the Institutional Board Review. Samples originated from subjects from arthroscopy interventions ($n = 25$, age range: 22–75 years, sex distribution: five females and 20 males) and autopsy ($n = 1$, 55-year-old male). Subjects from arthroscopy had been clinically diagnosed with meniscal tear. The subject from autopsy was free from any condition affecting the cartilage. Upon extraction, all samples were preserved in cold (5–10 °C) phosphate-buffered saline solution (PBS, Dulbecco's PBS solution 1 ×, no. 21-031-CV, Cellgro Mediatex, Herndon, VA, USA) and imaged with CM within the first 24 h. For each meniscus sample, mirror images from CM and conventional light microscopy were compared. Special care was taken to establish imaging correlation based on tissue microarchitectural patterns. No external marking agents such as ink were used so as to free the tissue from any exogenous substance that would distort the results. Among the 26 samples studied under light microscopy, one presented clinical findings consistent with gout and one presented clinical findings consistent with chondrocalcinosis.

CM imaging

To image the tissue, the samples were placed on a coverslip glass (Fisherbrand Coverglass 12545100, Fisher Chemical Company, Pittsburgh, PA, USA). PBS was used both as hydrating agent for tissue preservation and as immersion medium between the lens and the specimen. All meniscus specimens were imaged both in bulk and after radial and longitudinal manual sectioning with scalpel blades. For the present study, we used a commercialized near-infrared, reflectance confocal microscope (VivaScope 1999, Lucid Inc., Henrietta, NY, USA) based on a prototype constructed in our laboratory for imaging human skin *in vivo*. Detailed descriptions of the principles of CM and the particular design of our microscope have been reported elsewhere (Rajadhyaksha *et al.* 1995; Rajadhyaksha *et al.* 1999). With this imaging technique, tissues are illuminated with a low-power (30 mW at the level of the tissue), 830 nm diode laser. Objective lenses employed are water-immersion, 30 × and NA 0.9. Contrast in the images is obtained from the natural differences in refractive indices of the microstructures in the tissue. By convention, highly-refractile structures appear white on screen, while low-refractile structures appear black. CM images appear on a computer monitor in real time at 10 Hz, as the specimen is scanned in the x, y and z planes by the investigator. Typical resolution of this confocal microscope is 0.5–1 μm in the lateral axis and 2–4 μm in the vertical axis (section thickness) comparable to light microscopy. Z-axis resolution is about 4 μm. Depth of imaging typically reaches 150–300 μm below the tissue surface, depending on tissue composition. This confocal microscope has been classified by the FDA as a pathological type microscope and is cleared for imaging unstained tissue, *in vivo* or *in vitro* (CFR 21 no. 846–3600). A micron-graded standard was used as a reference for structure measurements in all our studies (Graticules, Pyser-SGI Ltd, Tonbridge, UK). CM imaging was performed first on PBS-hydrated samples and later on those same samples briefly exposed to 5% acetic acid (Heinz-brand table vinegar, 5% acetic acid content).

Histology procedures

Immediately after imaging with CM, meniscus samples were fixed in 10% phosphate-buffered formalin (Fisher Scientific 10% Buffered Formalin, SF 100–4, Fisher Chemical Company) and processed for routine histology. Four-micron thick sections were stained with haematoxylin and eosin. Additionally, specific staining for elastic fibres was performed following Verhoeff-Van Gieson's method. Specific nerve staining was performed with PGP 9.5 antibody (Rabbit anti-protein gene product 9.5 polyclonal antibody, Chemicon International, Temecula, CA, USA) (Wilson *et al.* 1998). Histology preparations were examined under conventional and cross-polarized light microscopy (Zeiss Axiophot 1, Zeiss Axiopath Systems, Carl Zeiss MicroImaging Inc., Thornwood, NY, USA).

Results

Examination of the present series of human meniscus samples under CM is subdivided into three different histological patterns: normal, degenerative disease and crystal deposition disease (chondrocalcinosis and gout).

Normal pattern

A normal pattern of CM imaging of human meniscus was seen in 19 samples. Two distinct layers were present. An upper, hyperefractile layer was densely populated by cells (Figure 1, arrowhead). This was followed by a deeper layer rich in fibre bundles and with scattered cells (Figure 1, star). Figure 1 shows a comparison between images of normal meniscus obtained by routine light microscopy, polarized light microscopy and CM.

With CM, cell morphology varies according to the plane of imaging. Meniscus cells are visualized as round or oval, hyporefractile structures (Figure 2, arrows). Cells are particularly numerous in upper layers (Figure 2, arrowheads), often appearing isolated or forming grouplets and less frequently, forming piles. When forming piles, their axis is perpendicular to that of the matrix striae (see below). Vertical sections of the meniscus exhibit superficial, oval cells found amidst the compact, hyperefractile matrix (Figure 2b, arrows). By contrast, images in horizontal planes display cells with round morphology (Figure 2c,d, arrows). Exposure of the tissue to acetic acid renders the nuclei more refractive, thus making them more easily distinguishable from the surrounding cytoplasm and extracellular matrix (Figure 2b,d, arrows). Nuclear sizes range from 7.5 to 11 μm.

The meniscus extracellular matrix is hyperefractile and heterogeneous (Figure 3). CM imaging in horizontal planes reveals an alternation of hyper- and hypo-refractile striae within the matrix, so that it conforms a zebra pattern (Figure 3b–d). This pattern is present throughout different imaging depths and does not vary upon the exposure of the tissue to acetic acid. Changes in size and orientation of these striae are seen when comparing superficial (Figure 3b) and deeper tissue layers (Figure 3c,d). These striae are sometimes intersected by thin, straight hyperefractile fibrous tracts (Figure 3d, arrow). A pattern similar to that of the zebra pattern is observed in haematoxyilin – eosin stained sections examined under cross-polarized light microscopy (Figure 4a).

Within the extracellular matrix, three types of fibres are identified with CM: circumferential fibres, radial fibres and thin fibres enhanced by acetic acid (Figure 4). Circumferential fibres are seen as highly refractive, wide fibrous tracts extending between both the meniscal horns (Figure 4b, arrows). Radial fibres and their thin branches are seen in vertical sections of the meniscus, constituting a complex network

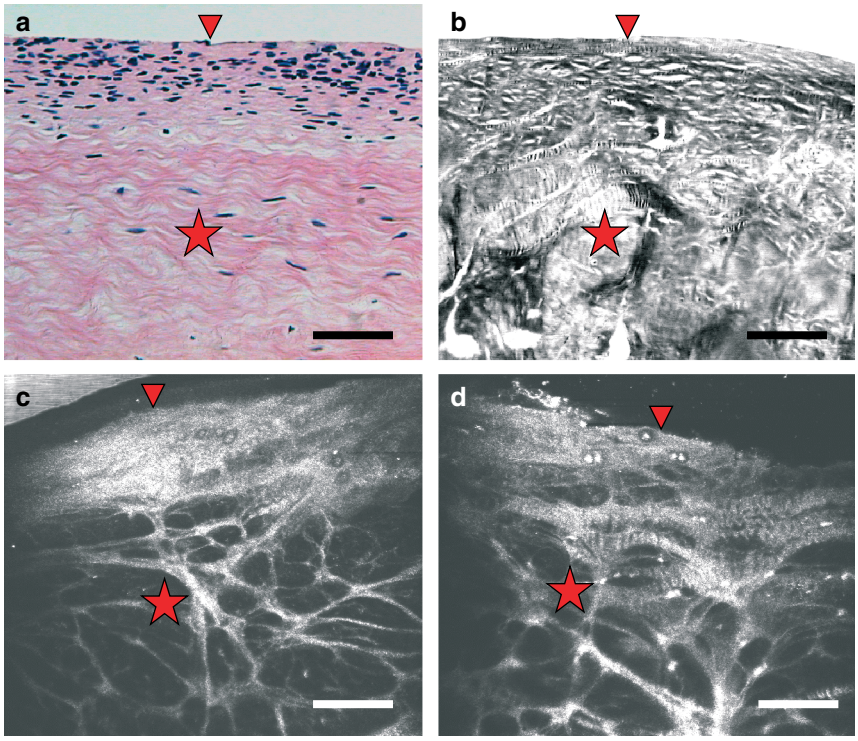

Figure 1 Comparison of vertical sections of human knee meniscus as seen with routine haematoxylin – eosin staining examined under light microscopy (a), cross-polarized light microscopy (b) and near-infrared reflectance confocal microscopy imaging of intact tissue exposed to phosphate-buffered saline (c) and to acetic acid (d). The densely cellular top layer (arrowhead) and the more fibrillar interior (star) are readily depicted in the four images. Scale bar represents 100 μm.

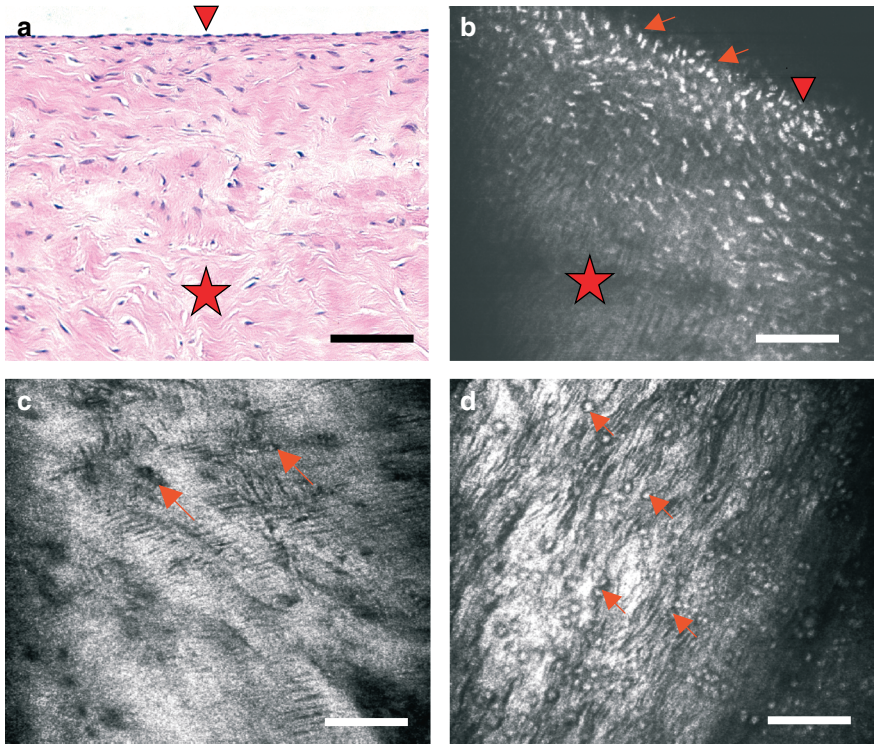

Figure 2 Meniscus cells as seen with light microscopy of haematoxylin and eosin-stained sections (a) and with near-infrared, reflectance confocal microscopy (CM) of bulk tissue (b–d). Vertical sections of meniscus (a and b) reveal that cells (arrows) are much more abundant in superficial layers (arrowhead) that in the interior of the meniscus (star). Near the surface, they exhibit an ovoid or fusiform morphology. Virtual sections of meniscus in horizontal planes with CM reveal cells of round morphology (c, arrows) and a surrounding hyperefractile matrix that exhibits fine striae. The location of cells is better seen when tissue is briefly exposed to acetic acid (d, arrows), which renders nuclei more refractive (white in the images). Scale bar represents 100 μm.

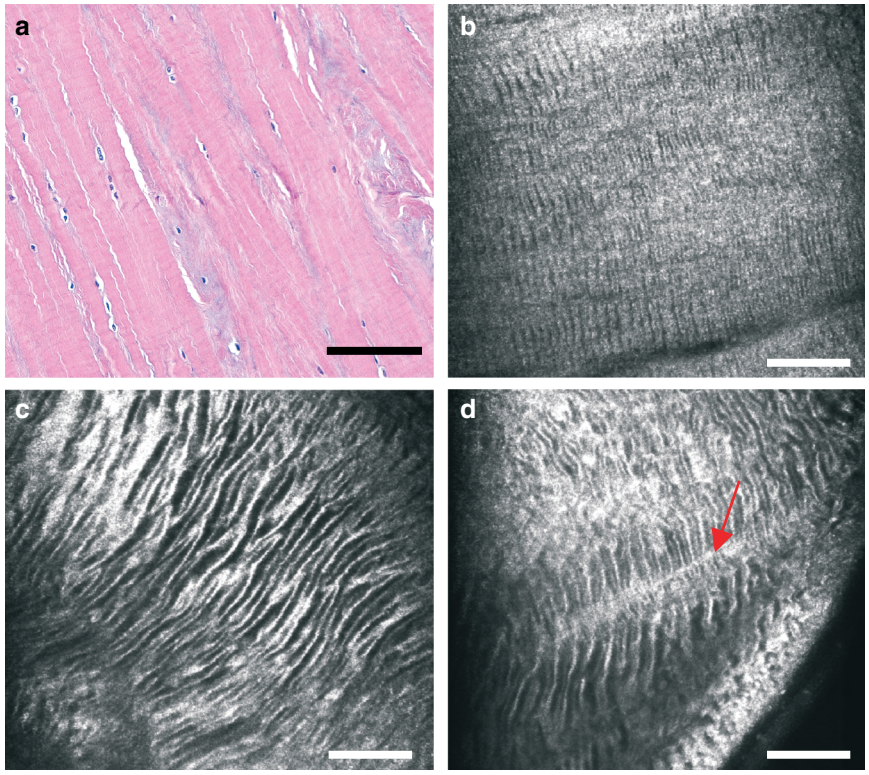

Figure 3 Meniscus matrix as seen with light microscopy (a) and with near-infrared, reflectance confocal microscopy (CM) (b–d). With CM, extracellular matrix appears generally hyperefractile, displaying hyporefractile striae that conform a zebra pattern. This zebra pattern is present both in the superficial (b) and in the intermediate-deep layers (c and d) of the meniscus, progressively increasing the width of its striae. Striae appear intersected by perpendicular fibrous tracts of greater refractility (d, arrow). Scale bar represents 100 μm.

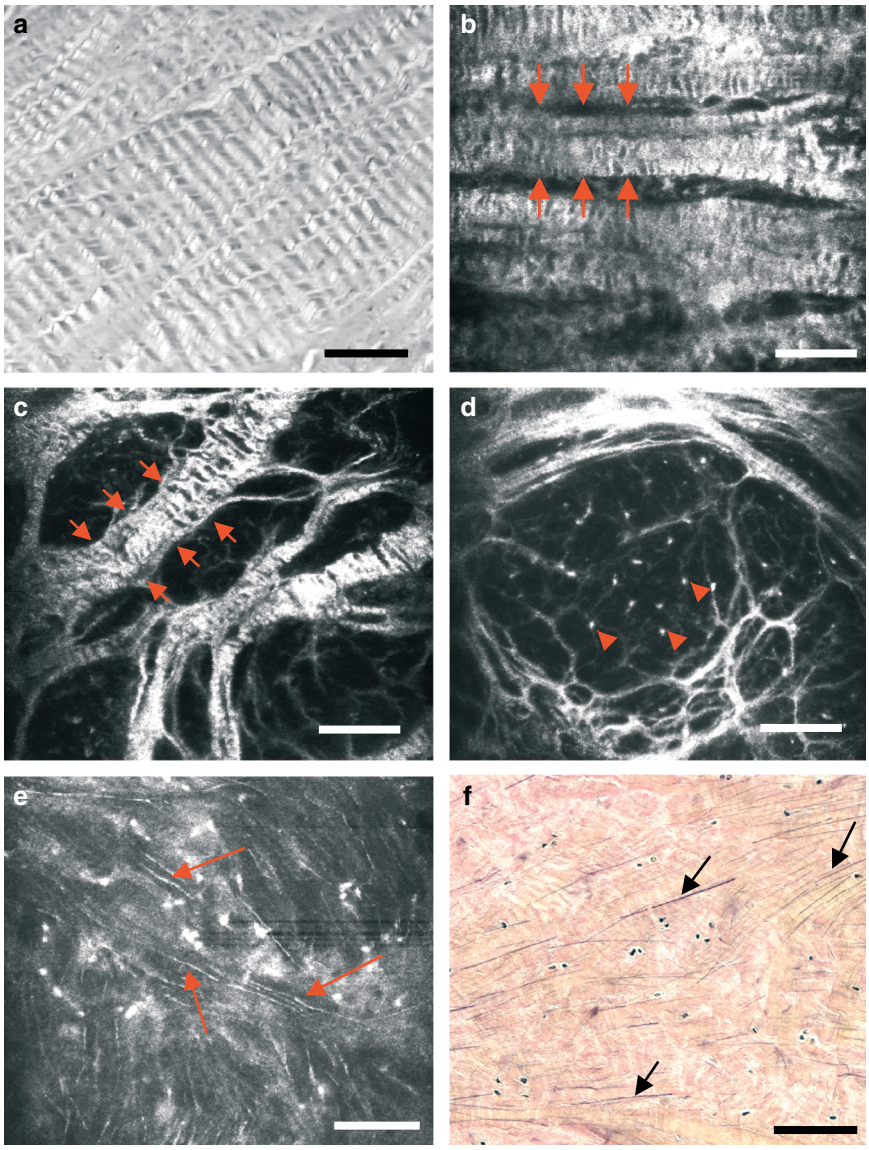

Figure 4 Meniscus fibres seen with polarized light microscopy (a), routine light microscopy (f) and near-infrared, reflectance confocal microscopy (CM) (b–e). Circumferential (b, between arrows) and radial fibres (c, between arrows) are readily seen with CM. Both types of fibres exhibit areas of zebra pattern. Brief exposure of the tissue to acetic acid highlights the presence of cell nuclei interspersed within the fibrous mesh (d, arrowheads), which were not clearly seen before acetic acid application. Acetic acid also reveals a third type of fibres in CM images (e, arrows). These thin fibres are orientated in different directions and correlate well with elastic fibres stained by Verhoeff-Van Gieson's method (f, arrows). Scale bar represents 100 μm.

(Figure 4c, arrows; Figure 4d). Fibre bundles display a wide range of sizes, with diameters ranging from 7 to 22.5 μm. In general, they are larger and form a tighter network towards the posterior horn of the meniscus. Both circumferential and radial fibres display areas of the aforementioned zebra pattern. The exposure of human meniscus to acetic acid highlights the presence of thin, short and straight fibres that follow random directions (Figure 4f, arrows). Their morphology and disposition correlate well with those of the elastic fibres stained by Verhoeff-Van Giesson's method (Figure 4e, arrows).

Neurovascular structures in human meniscus are also readily visualized with CM (Figure 5). Vessels are found in the most lateral area of the meniscus (the so-called red – white zone) (Figure 5a–d). CM images depict the three-dimensional disposition of these highly refractive structures of different sizes and sharp contour that penetrate from the lateral surface into the meniscal body. On the other hand, nerve endings appear as highly refractive, longitudinally striated structures of variable sizes (Figure 5e,f). These structures correlate well with those nerve endings stained with PGP 9.5 antibody in mirror histology sections and appear located alongside with the vessels, in the outer third of the meniscus body and the horns.

Degenerative disease pattern

The degenerative pattern was seen in five menisci and consists of an impairment in the cellular distribution described for

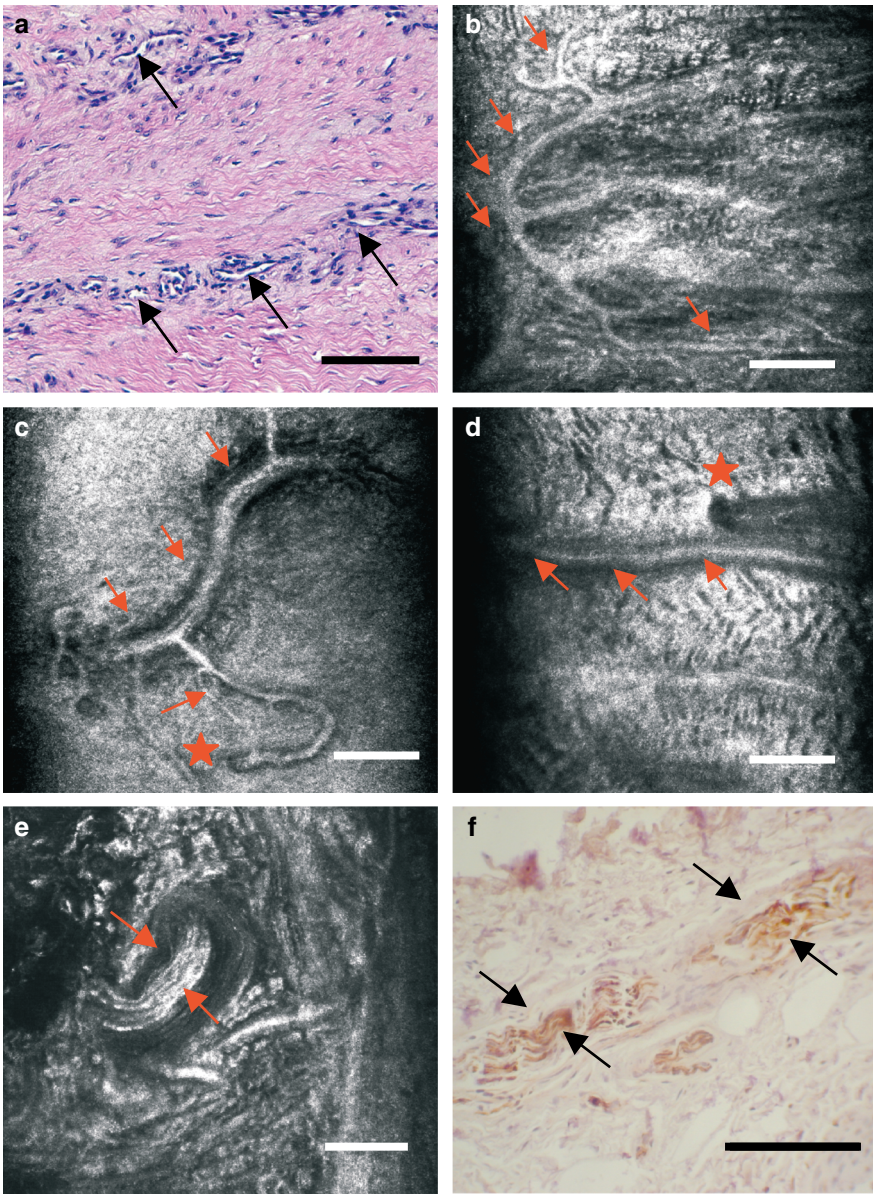

Figure 5 Neurovascular structures in the outer third of human knee meniscus, as seen with light microscopy (a and f) and with near-infrared, reflectance confocal microscopy (CM) (b–e). CM readily depicts the localization of vessels and the distribution of their branches (b–d, arrows). The points in which these vessels penetrate from the outer fringe of the meniscus may also be located with precision (d, star). Meniscal myelinated nerve endings are easily distinguishable for their hyperefractile, striated appearance (e, arrows). Images with CM correlate well with those from companion histology sections stained for PGP 9.5 antibody (f, arrows). Scale bar represents 100 μm.

normal meniscus, with the absence of the aforementioned cell gradient from surface to depth and a decrease in cell density (Figure 6a,b, arrows). In deeper planes, matrix architecture appears greatly disorganized and heteromorphic (Figure 6a,b, star). CM images show the presence of matrix fibre bundles (Figure 6c, arrows) and occasional sites of meniscal tear (Figure 6d, arrowhead).

Crystal deposition disease pattern

CM images show the three-dimensional disposition of crystal deposits in the two menisci from patients diagnosed with gout and chondrocalcinosis (pseudogout), respectively. In gout (Figure 7a–d), urate crystals can be visualized as multiple, highly refractive, needle-shaped structures of heterogeneous distribution (Figure 7a,b, arrowheads). The surrounding matrix shows increased refractility and disruption in its architecture, with fibres showing different sizes and orientations. Cells appear hypertrophic (Figure 7c, arrows). Aberrant vascular structures are also visualized within the tissue (Figure 7d, arrows).

In chondrocalcinosis (Figure 8a–f), calcium pyrophosphate dihydrate deposits appear in a patchy form and are visualized as large, hyperefractile globular masses amidst thinned matrix

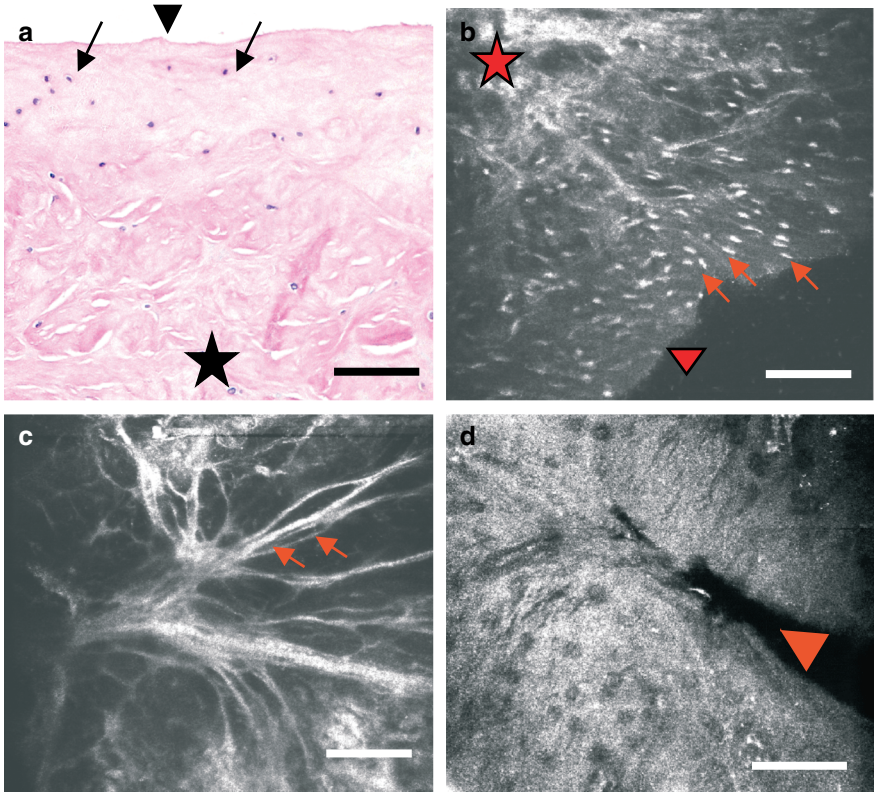

Figure 6 Human knee meniscus exhibiting a degenerative pattern, imaged with routine light microscopy (a) and with near-infrared, reflectance confocal microscopy (CM) (b–d). This degenerative pattern consists of an impairment in the cellular density and distribution, that is, an absence of the decreasing cell gradient from surface (a and b, arrowhead) to depth (a and b, star) described previously for normal meniscus. Matrix architecture appears greatly disorganized and heteromorphic, with thinned matrix fibre bundles (c, arrows) and occasional sites of meniscal tear (d, arrowhead). Scale bar represents 100 μm.

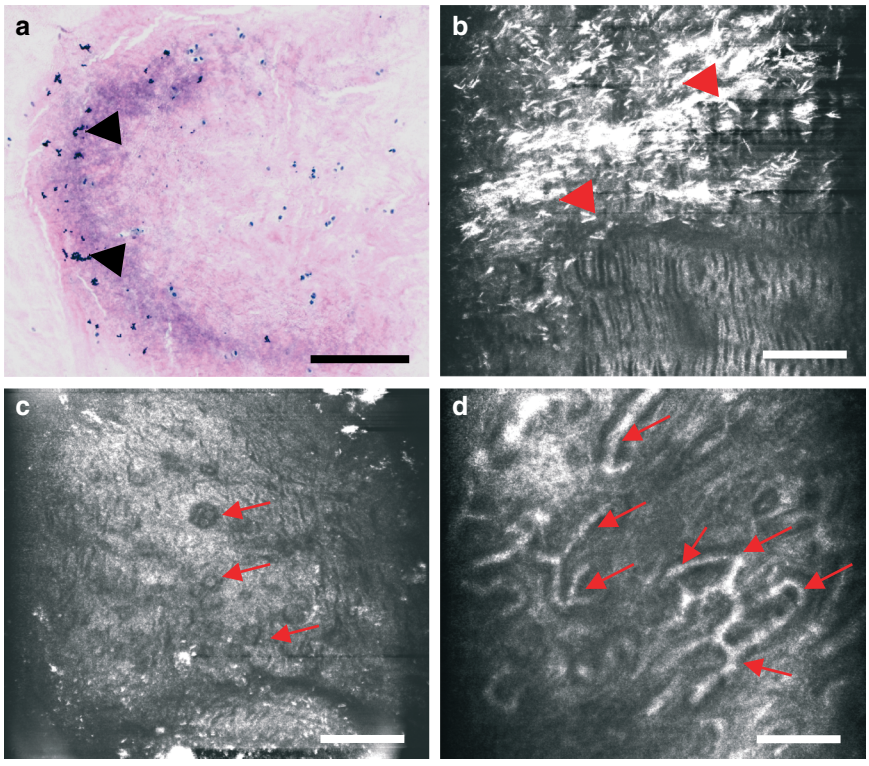

Figure 7 Human knee meniscus affected by gout imaged with routine light microscopy (a) and near-infrared, reflectance confocal microscopy (CM) (b–d). In CM images, urate crystals are visualized as multiple, highly refractive, needle-shaped structures of heterogeneous distribution (b, arrowheads). Note that these crystals inadvertently disappear when tissue is obtained and preserved in saline serum prior to routine histology processing (a, arrows). The surrounding matrix shows increased refractility and disruption in its architecture, with fibres showing different sizes and orientations. Cells appear hypertrophic and with a greater tendency to form clusters (c, arrows). Aberrant vascular structures are also visualized within the tissue (d, arrows). Scale bar represents 100 μm.

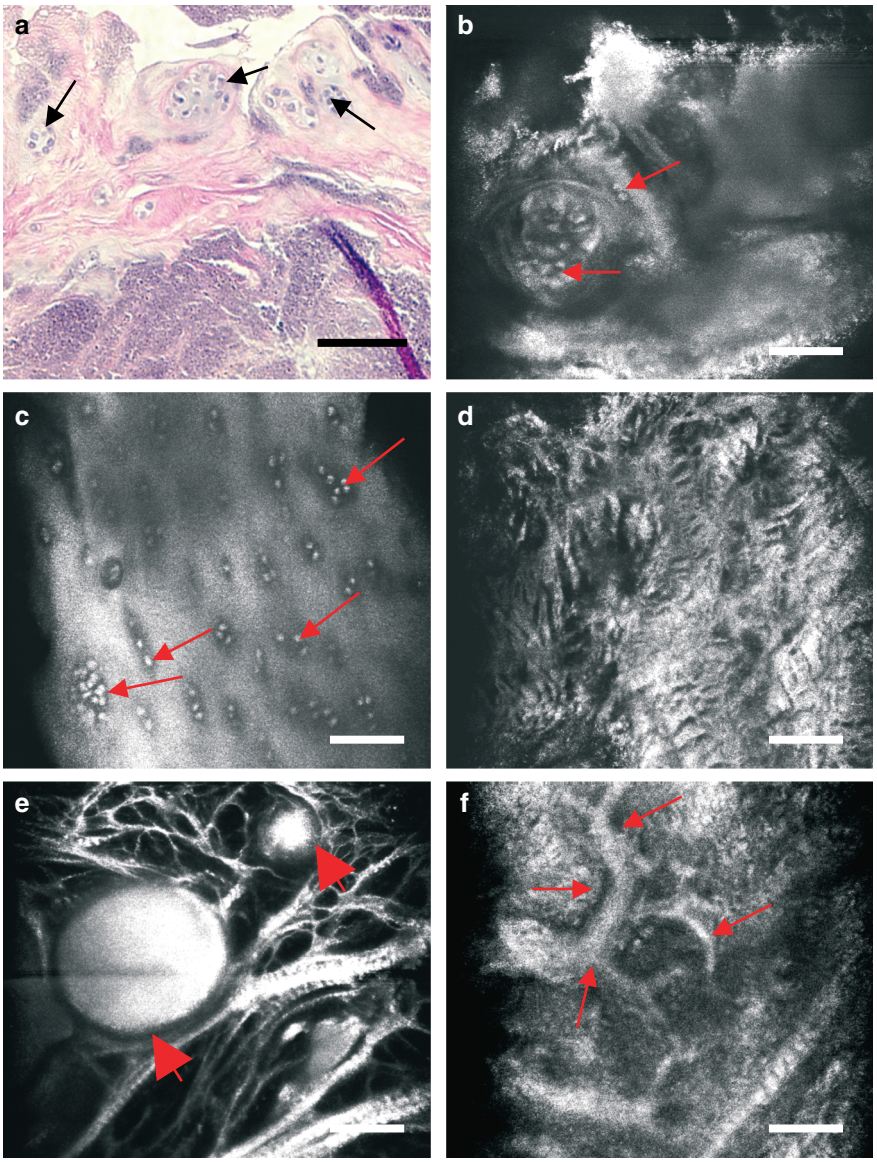

Figure 8 Human knee meniscus affected by chondrocalcinosis imaged with routine light microscopy (a) and near-infrared, reflectance confocal microscopy (CM) (b–f). Calcium pyrophosphate dihydrate deposits appear in a patchy form. CM reveals how the hypertrophic cells show a greater tendency to form clusters (a–c, arrows). The matrix also changes its morphology and refractility, appearing disorganized and devoid of the regular zebra pattern (d). Crystal deposits are visualized as large, hyperefractile globular masses (e, arrows) amidst thinned matrix fibres. The size of these deposits varies, with values ranging from 50 to 217 μm. Aberrant vascular structures are visualized within the tissue (f, arrows). Scale bar represents 100 μm.

fibres (Figure 8e, arrows). The size of these deposits vary, with values ranging from 50 to 217 μm. Cells appear enlarged and grouped in rows or clusters (Figure 8b,c, arrows). Extracellular matrix is distorted (Figure 8d), occasionally presenting aberrant vascular structures across it (Figure 8f, arrows).

Discussion

This is the first study using CM as an imaging tool for evaluating unprocessed human meniscus. Differences between normal and degenerative disease menisci were identified with CM, and the images were comparable to mirror histology sections. CM provides real-time histological information while preserving the native state of the meniscal tissue. CM images were comparable to mirror histology sections. Virtual sections of a bulk specimen can be obtained without inducing any change in the tissue and thus without interference with subsequent histological techniques performed on the same tissue sample. Furthermore, the possibility of screening large areas of tissues for areas of representative histological findings allowing subsequent traditional biopsy is another advantage. The three-dimensional architecture and biomechanical properties of human meniscus are thus amenable to study by CM. The results are similar to those obtained with CM when studying other unprocessed human tissues (González *et al.*

1999; White *et al*. 1999; White *et al*. 2000; Langley *et al*. 2001; Campo-Ruiz *et al*. 2002).

The structural anisotropy of native human meniscus is visualized readily with CM. Our images depict a highly cellular top layer and a more fibrous, intermediate-deep area in the bulk of the tissue. In hydrated tissue, oval-round shaped structures interpreted as chondrocytes appear less refractile than the surrounding extracellular matrix. Exposure to acetic acid renders nuclei highly refractile. This phenomenon of nuclei enhancement has been previously described in the literature for nuclei of epithelial cells (Drezek *et al*. 2000; Rajadhyaksha *et al*. 2001). It was postulated that acetic acid disrupts the bond between histones and DNA strands, after which DNA would clump and thus become more refractile. Testing whether other phenomena leading to nuclear shrinkage, such as apoptosis, also enhance nuclear refractility justifies further studies.

Regarding the matrix fibres, CM images clearly depict circumferential and radial fibres as they intersect and branch out. With routine histology processing, a retraction artefact might occasionally be responsible for the massive look of the matrix, as depicted in Figure 1a. In contrast, CM images of freshly excised, unprocessed meniscus show fibres distended in their native state, as in Figure 1c. Fibrocartilage collagen fibres are known to form either irregular bundles between the groups of chondrocytes, parallel alignments along the columns of chondrocytes or lamellae. Our work demonstrates the existence of circumferential fibres in both the internal and the middle circumferences of the meniscus, supporting some of the previous observations (Bullough *et al*. 1970; Aspden *et al*. 1985). Most importantly, CM imaging of vertical sections showed the presence of radial fibres throughout the whole of the meniscus, both in the surface and in the interior, as well as in medial and lateral areas. Additionally, we noted that radial fibres form a tighter network in middle and posterior areas of the meniscus, thus supporting published findings with polarized light microscopy (Skaggs *et al*. 1994).

The zebra pattern (Figure 3) described for the extracellular matrix depicted in CM images is probably because of an undulated, three-dimensional disposition of matricial collagen fibres and lamellae. The highly-refractile striae may correspond to the top part of an undulating collagen sheet and the dark striae to regions of the same sheet as it undulates outside CM virtual sections. We noted that the exposure to acetic acid did not change this appearance nor revealed the presence of any nuclei along the hyper- and hyporefractile striae. In samples examined, no correlation could be established between the presence of that zebra pattern and any particular age or sex group or any particular meniscal layer. This pattern was also observed in healthy pig menisci imaged by CM in our laboratory (data not shown). Thin sections examined under polarized light microscopy also reveal a similar zebra pattern. The undulated sheets of collagen fibres may contribute to the shock-absorbent properties of the knee meniscus, by deforming whenever stress or weight-bearing act on them (Yasui 1978). Because CM is entirely nondestructive, it is conceivable to observe deformation and failure of meniscus fibres and lamellae under mechanical stress, at the histological level.

A new and interesting finding was the presence of certain matrix fibres which enhance after exposure to acetic acid. These fibres appear short, straight and loose, with a random disposition throughout the tissue. Careful comparison between CM images and companion histology sections stained by Verhoeff-Van Gieson's method suggests that these could be elastic fibres, which are present in a small proportion in the meniscus extracellular matrix (Figure 4). Acetic acid may induce a conformational change in the fibres that increases their refractility. To our knowledge, the phenomenon of elastic fibre enhancement has not been previously described in the literature.

Vessels and nerve endings were seen with CM, without needing to use any specific stain, and it was possible to track their three-dimensional pathway within the meniscus outer layers. Our CM images show vessels only in the outer, lateral area of the specimens, confirming that the majority of the meniscal tissue is avascular and that only a peripheral third (the red zone) gets vascular supply from the geniculate plexus (Arnoczky & Warren 1982; Danzig *et al*. 1983). There are vessels of different sizes, with complex arrangement and branching, as they penetrate from that outer fringe, inwards. Because many of our specimens came from patients diagnosed with meniscal tear, the presence of these vessels may also be linked to that particular lesion and the repair process that starts to take place in some cases. CM is also a nondestructive imaging technique for myelinated nerves that enter the meniscus from the articular capsule and the cruciate ligaments. In our CM images, the highly-refractile, striated pattern correlates very well with that observed with immunohistochemical staining techniques for nerve tissue detection. Nerve endings are important for pain sensation whenever a meniscal tear occurs and also in the trophism of healing meniscal cartilage. Our morphological findings for the nerves are in agreement with previous studies using conventional sections and stains (Zimny 1988; Hirasawa *et al*. 2000; Mine *et al*. 2000).

With regard to the study of crystal deposition disease, our findings must be interpreted with caution because of the small number of samples. It appears however that CM may prove

useful in the distinction between types of crystal deposition and for imaging crystals that are lost inadvertently during preservation of the samples in PBS for routine histology staining. If this is confirmed, then CM may be both faster and more accurate for detecting crystal deposition in meniscal samples compared with traditional methods.

Therefore, CM has two main advantages. First, it provides real-time information and may be used *in vivo*. Because there is no need to cut, fix, embed, stain and set the specimen, much amount of time and resources are saved, and the whole study may be done in one single session. Second, it is not aggressive towards the tissue. CM needs no contrast agent to provide images. Thus, once the CM study has been performed, subsequent refined stainings for any modality of microscopy (light, electron, etc.) may be done.

However, it is important to note that CM has its limitations as an imaging technique. The major limitations are contrast among different structures, image definition and penetration depth. We have shown here that contrast limitations can be overcome partially by brief exposure of the tissue to acetic acid. Acetic acid did not induce significant morphological changes in the tissue, as confirmed by histology studies. However, acetic acid has been reported to induce apoptosis in cells, hence its implementation for *in vivo* studies is not risk-free (Ludovico *et al*. 2001). Thus, future studies of different contrast agents for CM are justified. The present CM images did not allow exact demarcation of plasma or nuclear membranes. In addition, there are small optical aberrations during CM that may distort true measurements and/or shapes of the structures. Spherical aberration exists because of mismatch of refractive indices between meniscus and the external fluid medium (PBS, in this study).

In summary, CM is a novel imaging technique for immediate, nondestructive, high-resolution optical sectioning through intact tissues. In this study, we describe CM imaging of meniscal architecture, with its blood and nerve supply in different spatial planes. This study also demonstrates the utility of CM in the distinction between normal and degenerative disease menisci in unprocessed tissue. Future applications of CM may include assessment of engineered tissue (cell implants viability, osteochondral allografts and autografts, etc.), superficial histological screening of any preserved meniscus allograft prior to its transplant, fast intraoperative diagnosis of neoplasia and inflammatory conditions or use during arthroscopy with miniature CM devices. In this regard, current efforts are being carried out to develop a fibre optic version of a confocal microscope (Tearney *et al*. 1998). This could provide an arthroscopic version of CM for *in vivo* assessments in the future.

Acknowledgements

The authors thank Mr John T. Demirs for his excellent preparation of the histology stained sections and Mr Steve Conley for his remarkable assistance in histology slide photography. This study was partially funded by Lucid Inc.

References

Arnoczky S.P., Warren R.F. (1982) Microvasculature of the human meniscus. *Am. J. Sports Med.* **10**, 90–95.

Aspden R.M., Yarker Y.E., Hukins D.W.L. (1985) Collagen orientations in the meniscus of the knee joint. *J. Anat.* **140**, 371–380.

Bullough P.G., Munuera L., Murphy J., Weinstein A.M. (1970) The strength of the menisci of the knee as it relates to their fine structure. *J. Bone Joint Surg.* **3**, 564–570.

Campo-Ruiz V., Ochoa E.R., Lauwers G.Y., González S. (2002) Human liver biopsy studied with near-infrared confocal microscopy. A pilot study. *Hum. Pathol.* **33**, 975–982.

Danzig L., Resnick D., Gonsalves M., Akeson W.H. (1983) Blood supply to the normal and abnormal menisci of the human knee. *Clin. Orthop.* **172**, 271–276.

Drezek R.A., Collier T., Brookner C. *et al.* (2000) Laser scanning confocal microscopy of cervical tissue before and after application of acetic acid. *Am. J. Obstet. Gynecol.* **182**, 1135–1139.

González. S., González. E., White W.M., Rajadhyaksha M., Anderson R.R. (1999) Allergic contact dermatitis: correlation of in vivo confocal imaging to routine histology. *J. Am. Acad. Dermatol.* **40**, 708–713.

Greis P.E., Bardana D.D., Holmstrom M.C., Burks R.T. (2002) Meniscal injury: I. Basic science and evaluation. *J. Am. Acad. Orthop. Surg.* **10**, 168–176.

Hirasawa Y., Okajima S., Ohta M., Tokioka T. (2000) Nerve distribution to the human knee joint: anatomical and immunohistochemical study. *Int. Orthop.* **24**, 1–4.

Langley R.G., Rajadhyaksha M., Dwyer P.J., Sober A.J., Flotte T.J., Anderson R.R. (2001) Confocal scanning laser microscopy of benign and malignant melanocytic skin lesions in vivo. *J. Am. Acad. Dermatol.* **45**, 365–376.

Ludovico P., Sousa M.J., Silva M.T., Leao C., Corte-Real M. (2001) Saccharomyces cerevisiae commits to a programmed cell death in response to acetic acid. *Microbiology* **147**, 2409–2415.

Mine T., Kimura M., Sakka A., Kawai S. (2000) Innervation of nociceptors in the menisci of the knee joint: an immunohistochemical study. *Arch. Orthop. Trauma Surg.* **120**, 201–204.

Pawley J., ed (1995) *Handbook of Biological Confocal Microscopy*, 2nd edn. New York: Plenum Press.

Rajadhyaksha M., González S., Zavislan J., Anderson R.R., Webb R.H. (1999) In vivo confocal scanning laser microscopy of human skin II: advances in instrumentation and comparison with histology. *J. Invest. Dermatol.* **113**, 293–303.

Rajadhyaksha M., Grossman M., Esterowitz D., Webb R.H., Anderson R.R. (1995) In vivo confocal scanning laser microscopy of human skin: melanin provides strong contrast. *J. Invest. Dermatol.* **104**, 946–952.

Rajadhyaksha M., Menaker G., Flotte T., Dwyer P.J., González S. (2001) Confocal examination of non-melanoma cancers in skin excisions to potentially guide Mohs micrographic surgery without histopathology. *J. Invest. Dermatol.* **117**, 1137–1143.

Skaggs D.L., Warden W.H., Mow V.C. (1994) Radial tie fibers influence the tensile properties of the bovine medial meniscus. *J. Orthop. Res.* **12**, 176–185.

Tearney G.J., Webb R.H., Bouma B.E. (1998) Spectrally encoded confocal microscopy. *Opt. Lett.* **23**, 1152–1154.

White W.M., Rajadhyaksha M., González S., Fabian R.L., Anderson R.R. (1999) Noninvasive imaging of human oral mucosa in vivo by confocal reflectance microscopy. *Laryngoscope* **109**, 1709–1717.

White M.W., Tearney G.J., Pilch B.Z., Fabian R.L., Anderson R.R., Gaz R.D. (2000) A novel non-invasive imaging technique for intraoperative assessment of parathyroid glands: confocal reflectance microscopy. *Surgery* **128**, 1088–1100.

Wilson T. ed (1990) *Confocal Microscopy*. San Diego: Academic Press.

Wilson P.O.G., Barber P.C., Hamid Q.A. *et al.* (1998) The immunohistochemical localisation of protein gene product 9.5 using rabbit polyclonal and mouse monoclonal antibodies. *Br. J. Exp. Pathol.* **69**, 91–104.

Yasui K. (1978) Three dimensional architecture of human normal menisci. *J. Jpn. Orthop. Assoc.* **52**, 391–399.

Zimny M. (1988) Mechanoreceptors in articular tissues. *Am. J. Anat.* **182**, 16–32.